Above-threshold ionization near the $3p4d\ ^1F^o$ autoionizing state in magnesium

A. Reber,[1] T. Baynard,[1] F. Martín,[2] H. Bachau,[3] and R. S. Berry[1]
[1]*Department of Chemistry and The James Franck Institute, The University of Chicago, Chicago, Illinois 60637, USA*
[2]*Departamento de Química C-9, Universidad Autónoma de Madrid, 28049 Madrid, Spain*
[3]*Centre des Lasers Intenses et Applications (UMR 5107 du CNRS-CEA-Université de Bordeaux 1), 351 Cours de la Libération, F-33405 Talence, France*
(Received 5 November 2004; published 9 May 2005)

Two-photon above-threshold ionization (ATI) relative cross sections from the $3\ ^1P$ state of Mg have been measured using two-color ionization in the focus of a magnetic bottle spectrometer and have been calculated using the Green's-function method in the Feshbach formalism and an L^2-integrable close-coupling approach, with a basis of L^2-integrable *B*-spline functions. We report these cross sections in the region of $3d4p\ ^1F^o$ autoionizing state, with photon energies of 3.3–3.6 eV. This is one of the few direct comparisons between *ab initio* theory and experiments in ATI in the vicinity of a Feshbach resonance. A good agreement between theory and experiment is found in the relative total cross sections.

DOI: 10.1103/PhysRevA.71.053402 PACS number(s): 32.80.Rm, 32.80.Dz

I. INTRODUCTION

Autoionizing states have been a central focus in the study of photon-atom and electron-atom dynamics. The presence of bound states in the continuum produces unique effects such as resonance stabilization, [1,2] and laser-induced continuum structure (LICS) [3], and even may induce a collapse of the Bose-Einstein condensate [4]. While numerous calculations have been performed to evaluate the positions and widths of these states [5–9], the number of comparisons between experiment and theory regarding resonances in Mg is strikingly rare [1,2]. In this study, we present both experimental and theoretical relative cross sections for the two-photon ionization of magnesium from the $3\ ^1P$ state in the region of the $3p4d\ ^1F^o$ autoionizing resonance, in which the second photon induces above-threshold ionization.

Above-threshold ionization (ATI) is a process in which an atom absorbs more than the minimum number of photons required to ionize the atom. The energy may then be transferred to the ejected electron or into exciting the ion [10]. The measurement of the relative ATI cross sections requires a tunable intense light source, a method of ensuring that all ionization processes are detected, and a method of characterizing the resulting processes. Calculating the cross sections by traditional methods is also difficult due to the continuum-continuum transition involved. These wave functions are not localized, and poles may be present in the intermediate-state transition amplitudes. Previous studies, experimental and theoretical, of ATI with Mg atoms have concentrated on the processes at high field intensities that induce multiphoton absorption of low-frequency, nonresonant radiation [11,12].

The experiment in this work is performed by crossing two laser beams and an effusive beam of magnesium atoms just inside the focus of a magnetic bottle spectrometer (MBS) [13]. One laser is tuned to populate the $3\ ^1P$ state in magnesium. The second laser beam is focused more narrowly, and the wavelength is scanned over the energy region of interest. This work is done in concert with another project, in which the low-energy photoelectrons undergo superelastic scattering by excited magnesium atoms [14–16]. In this process the electrons are produced by a one-photon process from the $3\ ^1P$ state and are consequently scattered in by an excited atom. Figure 1 shows the processes observed in these experiments, together with the relevant energy levels of magnesium.

ATI is a fundamental process in strong-field dynamics that is useful for investigating doubly excited states, shape resonances, and other resonant processes found in the continuum. It also represents a test of our ability to describe continuum-state processes. The continuum-continuum transitions are more difficult to evaluate than bound-continuum transitions because the wave functions are not localized and poles may be present in the intermediate-state Green's function. Our theoretical approach allows us to solve this problem in a simple way.

These calculations are performed using an L^2-integrable *B*-spline basis [17,18]. *B*-splines are sets of piecewise polynomials, which are capable of simultaneously representing bound and continuum states. We use the Green's-function

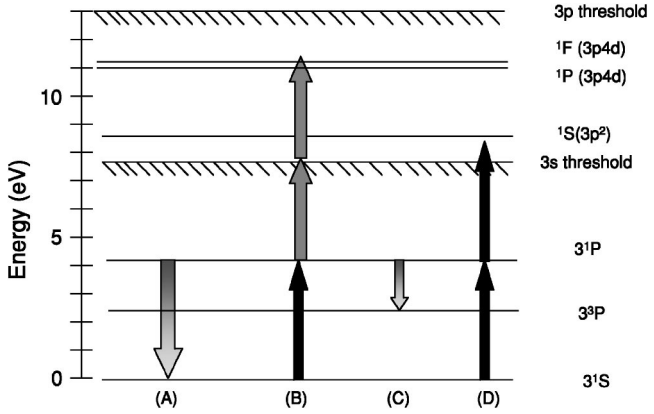

FIG. 1. A sketch of the relevant energy levels and processes studied in this paper. The dark arrows indicate the 285.21-nm light, the gray arrows indicate the nonresonant photons, and the shaded arrows indicate the deexcitation due to superelastic scattering.

method in the Feshbach formalism as described by Sánchez and Martín [19] and the L^2 close-coupling approach [20]. We work under the assumption of *LS* coupling and use lowest-order perturbation theory (LOPT). We are interested in the electronic structure of the Feshbach states, and we describe their positions, widths, and assignments. This method allows for a comprehensive study of the photoionization properties of Mg, including ATI.

There is a great deal of intrinsic interest in the ionization properties of Mg [1,2,5–7,9,21–23]. Karapangioti *et al.* have studied population trapping using three-photon ionization using both experiments and theory [1,2]. Two other experiments of interest are the works of Bonnanno *et al.* and Shao *et al.* who have studied doubly excited states in two-photon ionization of Mg [24,25]. Several theoretical studies have also been performed on Mg photoionization. Lyras and Bachau have studied phase control in two- and four-photon ionization in Mg [26]. Chang and Tang have studied atomic structure effects in three-photon ionization of Mg [23]. Luc-Koenig *et al.* have studied a variety of photoionization properties of Mg, including two-photon ATI [9]. Moccia and Spizzo and Mengali and Moccia studied one- and two-photon ionization of Mg using an L^2-integrable basis [5,21]. And in previous papers, the authors have studied two- and three-photon ATI in Mg [6,7].

In this work, we present a direct comparison of experimental and theoretical total relative cross sections for two-photon ATI from the $3\,^1P$ state of Mg. This is one of the only direct comparisons between experiment and *ab initio* theory in the region of a Feshbach resonance. In this case, we are examining the situation where the $3\,^1P$ state is prepared with a resonant photon source, followed by two-photon ionization where the first photon reaches the threshold. The widths and general behavior of the ionization cross section are studied as functions of photon energy. Because the experiments reveal both the ATI and superelastic scattering processes in the same observations, the discussion describes how these two processes can be unambiguously distinguished by their dependences on Mg density and laser intensity.

II. METHODS

The experimental apparatus and procedure have been described in detail elsewhere [14]. Briefly, the time-of-flight experiments are performed with a time-of-flight MBS [13] crossed with an effusive magnesium beam and two tunable dye lasers. One photon source is tuned to the $3\,^1P$ state of magnesium and the second is sharply focused for ionization and ATI. The two pulses are nearly collinear and aligned in time and space inside the focus of the MBS. All of the electrons are enclosed by an inhomogeneous magnetic field along a time-of-flight tube to a multichannel plate. The time interval between ionization and arrival at the detector is used to determine the energy of the electrons. The resonant radiation of wavelength 285.21 nm (4.35 eV) is created by a tunable dye laser pumped by a Nd:YAG laser operating at 20 Hz with a pulse duration of about 7 ns along with a KDP doubling crystal producing a laser intensity of approximately 1000 $\mathrm{W/cm^2}$ in the interaction region. The ionizing radiation is produced by XeCl excimer laser pumping a tunable dye laser operating from 3.3 to 3.575 eV at about 10^7 $\mathrm{W/cm^2}$. The absolute uncertainty in the photon energy is ±0.5 meV. The timing of the pulsed system is measured using a fast photodiode with a 100 ps rise time. The pulse duration for the resonant photon source is 6.4 ns, and the pulse length is 7.5 ns for the ionization source. The laser power is measured using a Molectron J4-05 laser meter monitoring a fraction of the beam, split from the main beam prior to its entering the vacuum chamber. The laser intensity dependences of the various electron peaks are measured by varying the laser intensity at constant magnesium density.

A resistively heated oven operating under effusive flow conditions is the source of the atomic Mg. The oven is operated between 650 and 850 K. The density of the atomic Mg vapor is determined using the photoionization signal from the prepared $3\,^1P$ state. The absolute cross section for photoionization from the $3\,^1P$ state with 285.21-nm photons is $8.1 \pm 2.3 \times 10^{-17}$ $\mathrm{cm^2}$ [27]. The atomic density is typically set to provide 1×10^{10} $\mathrm{atoms/cm^3}$ with 8% of the atoms in the excited state. Varying the temperature of the oven permitted the magnesium density dependence to be measured over an eightfold range.

Approximately 98% of the electrons ejected from the interaction region are collected by the MBS [28]. The MBS is a 4π steradian collecting version similar to Chesnovsky's version of the original design, except that we use a cobalt-samarium permanent magnet as the high-field source [29]. The high-field end of the MBS acts as a magnetic mirror reversing the velocity vectors of the electrons that are not initially moving toward the detector. The electrons travel down a 57-cm flight tube surrounded by the low-field solenoid. A cylindrical acceleration grid with a charge of 0.4 V is used to improve the collection efficiency of the threshold electrons produced by two-color resonantly enhanced multiphoton ionization (REMPI). Energy analysis is performed using time-of-flight (TOF) spectroscopy with the ionization laser pulse defining time zero. The detector is a dual chevron multichannel plate (MCP) which amplifies the signal. The pulses are sent to both a gated counter and a time-to-amplitude converter (TAC). The counter signal monitors the total electron count of a specific section of the TOF spectrum while the TAC signal measures the arrival time for the initial electron and allows for the energy analysis of the electrons. The time-of-flight peak profiles are due to the angular distribution and related time broadening of the electron trajectories within the MBS.

The multiphoton cross sections are evaluated in the dipole approximation for linearly polarized light. The cross section for a two-photon ionization process is given by

$$\sigma(\mathrm{cm^4\,s}) = C^{(2)}\omega^2 |M_{g\mu}^{(2)}|^2. \tag{1}$$

Here $C^{(2)}$ is a conversion from atomic to cgs units and is $2.505\,475 \times 10^{-52}$ $\mathrm{cm^4\,s}$, ω is the photon energy (a.u.), and $M^{(2)}$ is the amplitude associated with the multiphoton transition between the initial state g and the final channel μ in atomic units. For the two-photon case, the transition amplitude is found by

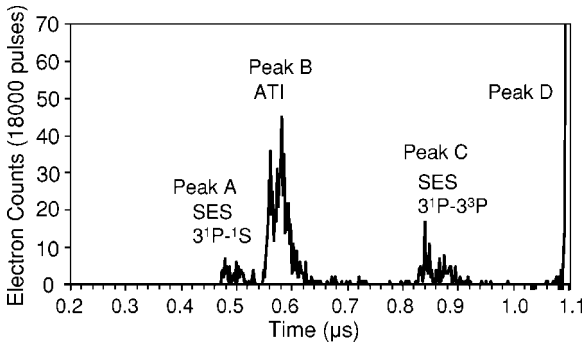

FIG. 2. A two-color time-of-flight spectrum. Peak *A* is caused by SES of electrons from $3\ ^1P$ Mg to $3\ ^1S$, peak *B* is caused by two-photon ATI from the $3\ ^1P$ state, peak *C* is caused by SES from $3\ ^1P$ to the $3\ ^3P$ state, and peak *D* is REMPI.

$$M_{g\mu}^{(2)} = \sum_{\nu} \frac{\langle g|\mathbf{D}\cdot\mathbf{e}|\nu\rangle\langle\nu|\mathbf{D}\cdot\mathbf{e}|\mu\rangle}{E_g+\omega-E_\nu} + \lim_{\eta\to 0^-}\int dE_\nu \frac{\langle g|\mathbf{D}\cdot\mathbf{e}|\nu\rangle\langle\nu|\mathbf{D}\cdot\mathbf{e}|\mu\rangle}{E_g+\omega-E_\nu-i\eta}. \quad (2)$$

Here, ν represents all possible intermediate (bound and continuum) states, g represents the ground state, **D** is the dipole operator, and **e** is the polarization vector. The velocity gauge of the dipole operator is used throughout this calculation. The discretization is then done by varying the box size to ensure that the energies for the true continuum state associated with the pole and its discrete representation match precisely. The intermediate-state wave functions were calculated using the L^2-integrable close-coupling method as developed by Cortés and Martín [20]. In this method, the multichannel continuum is transformed into a sum of single-channel continua or orthogonal uncoupled continuum states. The single channels are found by diagonalizing the Hamiltonian in a basis of two-electron configurations. The coupling of the channels is introduced through the Green's function.

The final continuum states are treated in the Feshbach formalism [30], using the method developed by Sánchez and Martín [19]. In this method, the resonant and nonresonant contributions to the wave functions are calculated separately because, to include electron correlation, it is easier first to compute the channels as uncoupled and then to couple the resonant and nonresonant channels together. The nonresonant configurations are selected by the *P* projection operator, and the doubly excited configurations are selected by the *Q* operator. This permits the evaluation of the widths and positions of the doubly excited states in a single calculation. It also clarifies the role of correlation in the spectra by identifying the Feshbach state and the weights of the contributing configurations. Further details of this method are supplied in Refs. [6,7].

All necessary wave functions are represented in a basis of two-electron states constructed from a *B*-spline basis [19,20]. *B*-splines are an L^2-integrable basis so that this representation results in a discretization of the continuum [31]. For each angular momentum, a basis of 650 *B*-splines of order 10 is placed in a linear knot sequence with the maximum radius

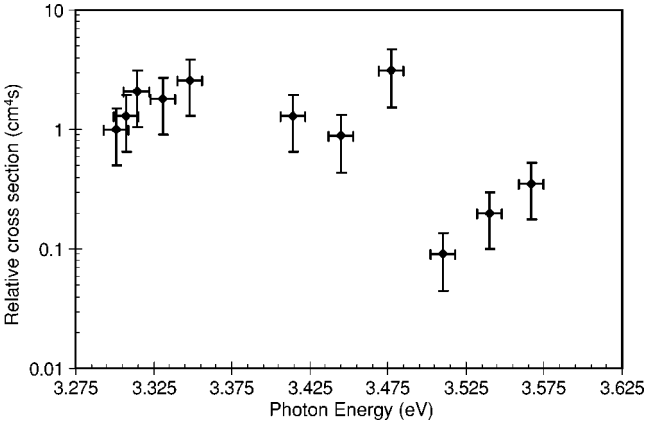

FIG. 3. Experimental relative cross sections as functions of photon energy.

of 250 a.u. The order of the basis refers to the number of nonzero basis functions at each radial point, except at the edge of the box where all basis functions are removed which do not conform to the boundary conditions. The basis is large enough that the energy levels and cross sections are essentially invariant to small changes in the size of the box and the basis. The Mg^{2+} core is represented by an analytical model potential that reproduces the valence-core potential resulting from self-consistent calculations, plus a phenomenological potential that represents polarization of the core. Details of this model potential can be found in Moccia and Spizzo [32]. The one-electron states are found by diagonalizing the Mg^+ Hamiltonian using the above *B*-spline basis set; this diagonalization is performed by imposing orthogonality with the core. The two-electron states are evaluated in a basis of configurations built from the one-electron spline-based orbitals. The number of two-electron configurations is typically 100 for uncoupled continuum states and 500 for bound and AIS states, and includes angular momenta up to $l=4$. The bound-state wave functions were calculated using the same one-electron basis as the continuum states.

III. RESULTS

In the experiments, two high-energy processes are observed. The first is ATI from the $3\ ^1P$ state (process (B) in Fig. 1):

$$\mathrm{Mg}^*(3\ ^1P) + 2h\nu_{nr} \rightarrow \mathrm{Mg}^+ + e^-_{peak\ B}, \quad (3)$$

where $h\nu_{nr}$ (3.30–3.575 eV) represents the nonresonant photons; the 3*s* threshold lies at 3.300 eV for the first photon. The resonant laser induces a significant population of the $3\ ^1P$ state at 4.35 eV above the fundamental state. The second process is a superelastic scattering (SES) process where a threshold electron collision with an excited magnesium atom results in the deexcitation of the atom. This process generates two peaks in the electron energy spectrum, due to the deexcitation of the $3\ ^1P$ both to the $3\ ^3P$ state and to the ground state, as shown by processes (A) and (C) in Fig. 1, and reactions (4) and (5), respectively:

TABLE I. Ionization rates as functions of Mg density for peaks *A*, *B*, and *C* with 374.45-nm light for the nonresonant ionizing source. The different ρ_i's indicate different Mg densities where measurements were taken. All numbers have been renormalized so that $\rho_1=1$. Boldface type indicates a linear dependence on density.

	Mg Density Dependence		
	ρ_1	ρ_2	ρ_3
REMPI	1.0	**2.3±0.2**	**8.0±0.8**
Peak *A*	1.0	3.1±0.4	49±5
Peak *B*	1.0	**2.3±0.3**	**8.5±0.8**
Peak *C*	1.0	4.4±0.3	50±5

$$\mathrm{Mg}^*(3\,^1P) + e^-_{thresh} \rightarrow \mathrm{Mg}(3\,^1S) + e^-_{peak\ A} \quad (4)$$

or

$$\mathrm{Mg}^*(3\,^1P) + e^-_{thresh} \rightarrow \mathrm{Mg}^*(3\,^3P) + e^-_{peak\ C}. \quad (5)$$

The electrons scattered in reactions (4) and (5) are produced by two-color REMPI of a different Mg atom as in Eq. (6):

$$\mathrm{Mg}^*(3\,^1P) + h\nu_{nr} \rightarrow \mathrm{Mg}^+ + e^-_{thresh}. \quad (6)$$

A characteristic time-of-flight spectrum of the electrons generated in the two-color-electron time-of-flight spectrum is shown in Fig. 2. Peak *B* corresponds to two-photon ionization of magnesium from the $3\,^1P$ state, where the first photon reaches the continuum and the second is above-threshold ionization. The two-photon ionization processes from the $3\,^1P$ state (i.e., three-photon one-color ionization from the ground state of Mg) including the resonant photon are not observed at the (resonant) laser intensity of this figure. Peaks *A* and *C* correspond to the superelastic scattering of the two-color REMPI electrons from the $3\,^1P$ state to the $3\,^1S$ and $3\,^3P$ states, respectively. Peak *D* is described by one-color REMPI.

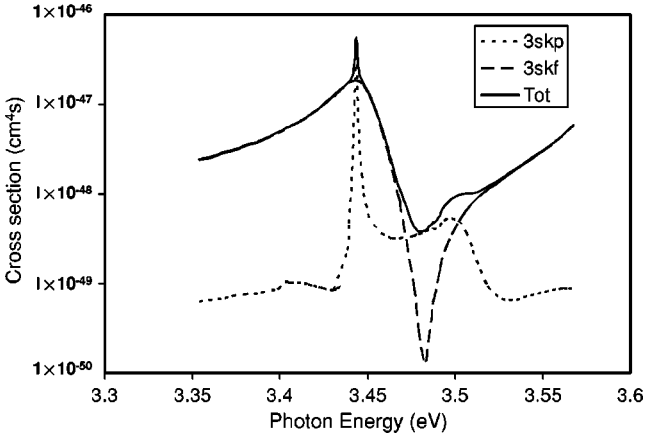

FIG. 4. Theoretical cross sections as a function of photon energy.

The density dependences of peaks *A*, *B*, and *C* are shown in Table I. The density of the $3\,^1P$ state was determined using the REMPI signal; therefore, the density dependence of the REMPI signal may then be treated as proportional to the density of the $3\,^1P$ state at constant resonant laser intensity. Peak *B* has the same dependence as REMPI, indicating a linear dependence on the $3\,^1P$ density and confirming the ATI assignment. Peaks *A* and *C* show a quadratic dependence on the Mg density, which is consistent with the occurrence of two different processes, each involving two Mg atoms, as required here for superelastic scattering. Table II shows the laser intensity dependence on the resonant

TABLE II. Relative electron count rates as a function of resonant and nonresonant (374.45-nm) laser intensity for peak *A*, *B*, and *C*, and REMPI. All rates have been normalized to the lowest laser intensity. Boldface type indicates a result consistent with ATI: a linear dependence on the population of the $3\,^1P$ state and quadratic dependence on the nonresonant photon intensity. Here, ρ_{Mg^*} and $(\rho_{\mathrm{Mg}^*})^2$ indicate the calculated population of the $3\,^1P$ state using Eq. (17) from Ref. [12] and the square of the population as a function of resonant laser intensity.

Resonant laser dependence				
Intensity (W/cm^2)	600±60	1060±100	1680±170	2360±240
ρ_{Mg^*}	1.0	**1.5±0.1**	**2.0±0.2**	**2.3±0.2**
$(\rho_{\mathrm{Mg}^*})^2$	1.0	2.4±0.4	4.0±0.4	5.2±0.5
Peak *A*	1.0	2.3±0.2	3.6±0.2	4.7±0.5
Peak *B*	1.0	**1.3±0.1**	**1.8±0.3**	**2.1±0.2**
Peak *C*	1.0	2.6±0.3	3.7±0.3	4.6±0.5
Nonresonant laser dependence				
Intensity ($\times 10^6$ W/cm^2)	6.3±0.6	10±1	21±2	
Relative intensity	1.0	1.6±0.2	3.2±.3	
REMPI	1.0	1.8±0.2	3.5±0.4	
Peak *A*	1.0	1.5±0.2	3.6±0.3	
Peak *B*	1.0	**2.7±0.3**	**8.6±0.8**	
Peak *C*	1.0	1.4±0.2	3.4±0.3	

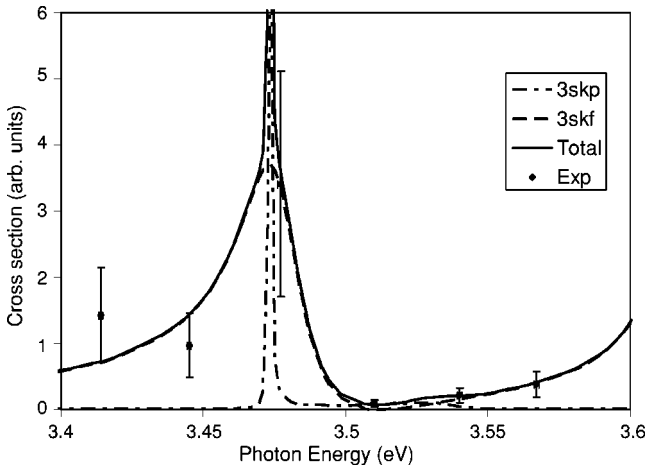

FIG. 5. A comparison of experimental and theoretical results. The theory has been shifted by 0.04 eV to compare the behavior.

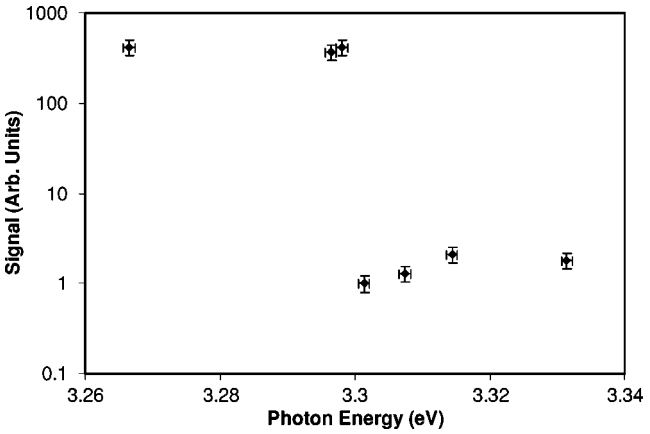

FIG. 6. The energy dependence of three-photon absorption for atomic Mg as a function of photon energy. The 3*s* threshold lies at 3.3004 eV above the $3\ ^1P$ state.

285.21-nm laser. The table shows that the intensity of peak *B* is proportional to the population of the $3\ ^1P$ state. This shows that Peak *B* is consistent with a one-resonant-photon process, as would be expected for a one-resonant-photon and two-nonresonant-photon process. Peaks *A* and *C* are consistent with two-resonant-photon processes as both the excited scattering state and the REMPI electron which is scattered require a resonant photon. Table II also shows the intensity dependence on the nonresonant laser (374.45 nm). These results show that peak *B* is dependent on two nonresonant photons, and peaks *A* and *C* have the same dependence as REMPI. These results conclude our characterization of peak *B*, showing that it is due to ATI.

Figure 3 shows the experimental ATI data in the energy region of interest. The signal rises slowly from the 3*s* threshold in the second photon at 3.3 eV. A mild dip in the cross section occurs between 3.35 eV and 3.43 eV. There is a significant jump in the cross section near 3.45 eV. This corresponds to the appearance of the $3p4d\ ^1F^o$ autoionizing state (AIS). The $3p4d\ ^1P^o$ AIS is also in this region; however, the $^1F^o$ resonance is much wider, so the observed resonance is probably due to the $^1F^o$ AIS. At energies just beyond this resonance, there is a pronounced transparency at about 3.5 eV with the cross section rising up from its minimum to 3.60 eV, the highest energy studied. The drop in the cross section is greater than an order of magnitude and is the most striking feature of the experimental data.

Only the relative energy dependence is provided here because of large uncertainties associated with the absolute intensity of the ionization source. The relative uncertainty is estimated at 50%. The primary source of this uncertainty is related to fluctuations in the laser timing system. The fluctuations lead to incomplete overlap of the two laser systems, resulting in nonideal ionization conditions. Additional factors include the uncertainty in the Mg density and uncertainty in the MBS efficiency. The laser intensity of the ionization source is estimated to be 10^7 W/cm^2. This results in a cross section of $10^{-48\pm2}$ cm^4 s for two-photon ionization from the $3\ ^1P$ state for 3.3-eV photons. This value is in agreement with the calculations in Fig. 4.

Figure 4 shows theoretical results for the two-photon ionization from the $3\ ^1P$ state. It is seen that the dominant channel is the 3*skf* channel, except in the region of the $3p4d\ ^1P^o$ AIS, where the cross sections of the two channels are comparable. The total and 3*skf* channels rise gradually from the 3*s* threshold in the second photon to the summit of the $3p4d\ ^1F^o$ AIS. The widths and dominant configurations of the $3d4p\ ^1F^o$ and $3d4p\ ^1P^o$ AIS are shown in Table III. The $^1F^o$ AIS is significantly wider, with a width of 49 meV, while the width of the $^1P^o$ AIS is 0.11 meV. Following the $3d4p\ ^1F^o$ AIS, the cross section of the 3*skf* channel drops sharply into a transparency. In the region of the transparency, the 3*skf* channel's cross section drops so that the cross sections of both the 3*skp* and 3*skf* channels are comparable. The 3*skf* channel then rises out of the transparency at 3.475 eV.

The combined plot in the region of the $3p4d\ ^1F^o$ AIS is shown in Fig. 5. The correspondence between theory and experiment is reasonable in the region of the resonance. Both theory and experiment show a relatively gradual rise in the total cross section followed by a sharp transparency. Following the transparency, the cross section rises monotonically. There is a slight disagreement in the exact position of the AIS. Our experiments place the AIS at 3.48 ± 0.03 eV, while the theory places it at 3.447 eV. Table IV summarizes previ-

TABLE III. Table of widths and the dominant configurations and dominant CI coefficients of the relevant AIS.

Resonance	Width (eV)			
$3p4d\ ^1F^o$	$\Gamma_{3p4d\ ^1F^o}=0.049$	$3p5d=0.8084$	$3p6d=-0.493$	$3p4d=-0.31$
$3p4d\ ^1P^o$	$\Gamma_{3p4d\ ^1P^o}=0.00011$	$3p4d=0.799$	$3p3d=-0.55$	$3p5d=-0.21$

TABLE IV. The position of AIS using two-photon ionization from the $3\,^1P$ state. The first two columns are for theory and experiments from the present work, the third is theory from Fang and Ho [8], next is Mengali and Moccia [21], and the last is the experiments of Rassi *et al.* [33].

Resonance	Theory (eV)	Expt. (eV)	Theory [8]	Theory [21]	Expt. [33]
$3p3d\,^1F^o$	3.135		3.141	3.144	3.34
$3p4d\,^1F^o$	3.447	3.48 ± 0.03	3.448	3.448	3.54
$3p4d\,^1P^o$	3.442			3.442	3.53

ous studies of the position of the $3d4p\ ^1F^o$ AIS. Previous experiments by Rassi *et al.* [33] place the AIS at 3.54 eV, while all of the theory studies are clustered tightly around 3.448 eV. This suggests a slight disagreement of theory and experiments although it is at the edge of the uncertainty in our experiment. The most likely explanation for this is that the frozen core approximation used in these calculations is inadequate to calculate the positions to a high degree of accuracy [32]. Furthermore, the experiments suggest the existence of a dip in the cross section between the threshold and area around the $3p4d$ AIS's that is not reproduced by the theory. In any case, the theory and experiments show a general reasonable agreement in the energy dependence of the two-photon ATI process.

An additional interesting feature of this work is the discontinuity in the cross section as the photon energy breaches the ATI threshold, as shown in Fig. 6. The transition here appears as the energy of the first photon to excite the $3\,^1P$ state moves from reaching a Rydberg state of Mg to populating a low-energy continuum state above the $3s$ threshold. The signal has been normalized to data for the lowest-energy ATI process. The relative intensity of the signal from the non-ATI multiphoton process is 400-fold greater than that of ATI. This behavior is certainly related to the fact that the coupled two-state dynamics is modified when the dominant ionization process of $3\,^1P$ Mg switches from two-photon absorption to one-photon absorption; the latter channel induces a strong loss of population, suggesting there a lower proportion of $3\,^1P$ in the ATI process. Other possible origins could include the influence of the $3p3d\ ^1F^o$ AIS, which is excited from the $3\,^1P$ state through the absorption of two photons of energy close to 3.3 eV. Also, the presence of the $3p^2\ ^1D^o$ perturber below the $3s$ threshold could add to this effect, and the influence of the one-color REMPI on the $3\,^1P$ population needs to be taken in account as well. A full understanding of the processes occurring at threshold is outside the scope of the present paper; it is in need of further theoretical and experimental developments.

IV. CONCLUSIONS

We have studied the two-photon ionization of Mg from the $3\,^1P$ state in the region of the $3d4p\ ^1F^o$ and $3d4p\ ^1P^o$ autoionizing states using an L^2-integrable B-spline basis for the calculation and experimentally by measuring electron energies with a magnetic bottle spectrometer. This combination of experiment and theory shows that the L^2-integrable B-spline method can accurately predict the behavior of the cross section in the region of an AIS. This is one of the relatively rare direct comparisons for such processes that use both experiment and *ab initio* theory. The improved detection capabilities using a MBS and a resonant transition allow measurements to be directly compared with theory. The position of the AIS was reasonably well located, although some improvement here might be desirable. Our theoretical results agree fairly well with all previous theoretical calculations, where they can be compared. It is possible that the frozen core assumption plays a role in this issue, as this and all previous calculations use a frozen core. The characterization of the resonance is straightforward, and a transparency at 3.50 eV was found by both theory and experiment. The TOF peaks in the electron energy spectrum are characterized to be two-photon ATI from the $3\,^1P$ state and superelastic scattering of the REMPI electrons from the $3\,^1P$ state to the ground state and to the $3\,^3P$ state. A discontinuity in the three-photon ionization rate was found at the ATI threshold. The theory also predicted the general behavior above the ATI threshold, although this region is the one in which the theory is likely to have the most difficulty.

ACKNOWLEDGMENTS

This work was supported by the National Science Foundation, GAANN (A. R.), and a National Science Foundation grant (T. B.). Additional support came from the U.S. Department of Education, Ministerio de Educacion y Ciencia (Spain) Project No. BFM2003-00194, and the D26 European COST action.

[1] N. E. Karapanagioti, O. Faucher, Y. L. Shao, D. Charalambidis, H. Bachau, and E. Cormier, Phys. Rev. Lett. **74**, 2431 (1995).

[2] N. E. Karapanagioti, D. Charalambidis, C. J. G. J. Uiterwaal, C. Fotakis, H. Bachau, I. Sánchez, and E. Cormier, Phys. Rev. A **53**, 2587 (1996).

[3] Y. L. Shao, D. Charalambidis, C. Fotakis, Jian Zhang, and P. Lambropoulos, Phys. Rev. Lett. **67**, 3669 (1991).

[4] E. A. Donley, N. R. Claussen, S. L. Cornish, J. L. Roberts, E. A. Cornell, and C. E. Wieman, Nature (London) **412**, 295

(2001).
[5] R. Moccia and P. Spizzo, J. Phys. B **21**, 1121 (1988).
[6] A. Reber, F. Martín, H. Bachau, and R. S. Berry, Phys. Rev. A **65**, 063413 (2002).
[7] A. Reber, F. Martín, H. Bachau, and R. S. Berry, Phys. Rev. A **68**, 063401 (2003).
[8] T. K. Fang and Y. K. Ho, J. Phys. B **32**, 3863 (1999).
[9] E. Luc-Koenig, A. Lyras, J. M. Lecomte, and M. Aymar, J. Phys. B **30**, 5213 (1997).
[10] P. Agostini, F. Fabre, G. Mainfray, G. Petite, and N. K. Rahman, Phys. Rev. Lett. **42**, 1127 (1979).
[11] D. Kim, S. Fournier, M. Saeed, and L. F. DiMauro, Phys. Rev. A **41**, 4966 (1990).
[12] X. Tang, T. N. Chang, P. Lambropoulos, S. Fournier, and L. F. DiMauro, Phys. Rev. A **41**, 5265 (1990).
[13] P. Kruit and F. H. Read, J. Phys. E **16**, 313 (1983).
[14] T. Baynard, A. Reber, S. Darveau, R. Niedziela, B. Prutzman, and R. S. Berry (unpublished).
[15] S. Darveau and R. S. Berry, in *Resonance Ionization Spectroscopy*, edited by J. C. Vickerman, I. Lyon, N. P. Lockyer, and J. E. Parks (AIP, Woodbury, 1998), p. 253.
[16] R. S. Berry, Phys. Chem. Chem. Phys. **7**, 286 (2005).
[17] C. De Boor, *A Practical Guide to Splines* (Springer, New York, 1978).
[18] H. Bachau, E. Cormier, P. Decleva, J. Hansen, and F. Martín, Rep. Prog. Phys. **64**, 1601 (2001).
[19] I. Sánchez and F. Martín, Phys. Rev. A **44**, 7318 (1991).
[20] M. Cortés and F. Martín, J. Phys. B **27**, 5741 (1994).
[21] S. Mengali and R. Moccia, J. Phys. B **29**, 1597 (1996).
[22] N. J. Kylstra, H. W. van der Hart, P. G. Burke, and C. J. Joachain, J. Phys. B **31**, 3089 (1998).
[23] T. N. Chang and X. Tang, Phys. Rev. A **46**, R2209 (1992).
[24] R. E. Bonanno, C. W. Clark, and T. B. Lucatorto, Phys. Rev. A **34**, 2082 (1986).
[25] Y. L. Shao, C. Fotakis, and D. Charalambidis, Phys. Rev. A **48**, 3636 (1993).
[26] A. Lyras and H. Bachau, Phys. Rev. A **60**, 4781 (1999).
[27] D. N. Madsen and J. W. Thomsen, J. Phys. B **35**, 2173 (2002).
[28] O. Chesnovsky, S. H. Yang, C. L. Pettiette, M. J. Craycraft, and R. E. Smalley, Rev. Sci. Instrum. **58**, 2131 (1987).
[29] T. Tsuboi, E. Y. Xu, Y. K. Bae, and K. T. Gillen, Rev. Sci. Instrum. **59**, 1357 (1988).
[30] H. Feshbach, Ann. Phys. (N.Y.) **19**, 287 (1962).
[31] O. K. Rice, J. Chem. Phys. **1**, 375 (1933).
[32] R. Moccia and P. Spizzo, Phys. Rev. A **39**, 3855 (1989).
[33] D. Rassi, V. Pejcev, T. W. Ottley, and K. J. Ross, J. Phys. B **10**, 2913 (1977).